Current Optics and Photonics
Vol. 3, No. 3, June 2019, pp. 243-247

ISSN: 2508-7266(Print) / ISSN: 2508-7274(Online)
DOI: https://doi.org/10.3807/COPP.2019.3.3.243

Compact, Wavelength-selectable, Energy-ratio Variable Nd:YAG Laser at Mid-ultraviolet for Chemical Warfare Agent Detection

Jae-Ihn Kim[1]*, Ki Ho Cho[1], Jae-Hwan Lee[2], and Yeon-Chul Ha[2]

[1]Laser and Sensor System Team, Hanwha Corporation, Seongnam 13488, Korea
[2]Agency for Defense Development, Daejeon 34186, Korea

(Received January 30, 2019 : revised May 7, 2019 : accepted May 7, 2019)

We have developed a compact, wavelength-selectable, Q-switched Nd:YAG laser at mid ultraviolet for chemical warfare agent detection. The fundamental wave at 1064 nm is delivered by a pulsed solid state laser incorporating with a square-type Nd:YAG rod in a resonator closed by two crossed Porro prisms for environmental reliability. The output energy at 213 nm (5ω) and 266 nm (4ω) by $\chi^{(2)}$ process in the sequentially disposed BBO crystals are measured to be 6.8 mJ and 15.1 mJ, respectively. The output wavelength is selected for 5ω and 4ω by a motorized wavelength switch. The energy ratio of the 5ω to the 4ω is varied from 0.05 to 0.85 by controlling the phase matching temperature of the nonlinear crystal for sum-frequency generation without change of the output pulse parameters.

Keywords : Ultra-violet, Raman spectroscopy, Q-switched Nd:YAG laser, Wavelength selectable
OCIS codes : (140.3610) Lasers, ultraviolet; (140.3540) Lasers, Q-switched; (300.6450) Spectroscopy, Raman

I. INTRODUCTION

Pulsed lasers in various spectral ranges are extensively used in applications, e.g. range finding for IR pulses [1], underwater object detection for visible pulses [2]. Ultraviolet (UV) lasers are widely employed for laser drilling [3], laser lithography [4], laser cooling of neutral atoms [5], and semiconductor inspections [6]. Furthermore, mid UV laser sources have served as efficient pumping sources for Raman spectroscopy with many advantages, e.g. the efficient separation of Raman signals from background fluorescence and a λ^{-4}-dependence of the Raman scattering cross section [7-12].

In particular, the mid UV radiation ranging from 200 nm to 300 nm has been used for chemical warfare agent (CWA) detection [13, 14]. Conventionally such UV photons have been delivered from gas lasers, e.g. a KrF laser for 248 nm and a frequency doubled Ar laser for 244 nm. But the application of such gas lasers with single output wavelength to detect CWAs is limited in use because of their bulky size, heavy weight, and maintenance issues involving periodic replacement of cooling water and excimer gas. Another UV light source is an optical parametric oscillator (OPO) based on a Nd:YAG laser able to widely tune the pump beam wavelength for potential resonance enhancement near allowed electronic transitions of the CWA molecules [15-17]. In OPO based light sources a resonant cavity is implemented so that the system configuration is complicated, and the laser system is sensitive to external perturbations, e.g. mechanical shock, which is a disadvantage in military applications.

In this article, we describe a compact, wavelength-selectable Q-switched Nd:YAG laser at mid ultraviolet for chemical warfare agent detection. The fundamental wave at 1064 nm is delivered by a Q-switched solid state laser interfacing with a square-type Nd:YAG rod in a resonator closed by two crossed Porro prisms for environmentally stable operation. The maximum output energy achieved per pulse is 153 mJ with a slope efficiency of 33%. The M-squared values in the horizontal and the vertical directions

*Corresponding author: sinerkim@hanwha.com, ORCID 0000-0002-6649-6868
Color versions of one or more of the figures in this paper are available online.

are deduced to be 2.4 and 1.7, respectively. The converted energies at 213 nm and 266 nm by $\chi^{(2)}$ process in the BBO crystals are measured to be 6.8 mJ and 15.1 mJ, respectively, by sequentially disposing the nonlinear crystals. The output wavelength is selected for 5ω and 4ω by a motorized wavelength switch. The energy ratio of the 5ω to the 4ω is varied from 0.05 to 0.85 by controlling the phase matching temperature of the nonlinear crystal for the sum-frequency generation on demand without change of the output pulse parameters, e.g. the width as well as the shape.

II. EXPERIMENTS AND RESULTS

Figure 1(a) shows the experimental schematic of the pulsed UV laser. The fundamental wave at 1064 nm is delivered by a Q-switched Nd:YAG laser with two crossed Porro prisms [18-20]. We use a squared Nd:YAG rod ($5 \times 5 \times 100$ mm^3) with the doping rate of 0.4 at.% as a gain medium in order to maximize thermal contact of the rod surface to the mechanical mount for efficient thermal dissipation. The square-type gain medium is pumped by a laser-diode array (LDA) in a crossed side-pumping configuration, where the half of the laser rod is pumped (cooled) in the left (right) side while another half side is pumped (cooled) in the right (left) side [21, 22]. The temperature of the LDA is controlled by a thermo-electric cooling (TEC) component to match the output wavelength of the LDA with the absorption peak of the Nd^{3+}-ions. The resonator is closed by the two crossed Porro prisms for environmentally stable operation. A Pockels cell ($LiNbO_3$) for Q-switching is inserted in the hold-off arm, and the second quarter-wave plate (QWP2) is appropriately rotated to compensate a phase shift induced by the Porro prism to accomplish hold-off during Q-switching. All the time sequences both for the LDA and the Pockels cell are precisely controlled by a main control board to generate giant pulses at the fundamental wave. The output coupling is achieved by rotating the first quarter-wave plate (QWP1) in the output-coupling arm in the resonator. The fundamental pulse energy out of the polarizer is reflected into the frequency-conversion stage.

The polarization of the fundamental wave is 90 degree rotated by a half waveplate to fulfill the phase matching condition for the second harmonic generation (SHG). A 15-mm-long type-I phase-matched BaB_2O_4 (BBO) crystal is employed for SHG. Both surfaces are anti-reflection (AR) coated for the fundamental wave and the frequency-doubled wave (2ω). After the first conversion both the ω and 2ω beams are incident on the second BBO crystal which is also type-I phase matched. The back reflection from the second BBO is much suppressed by an AR coating for ω, 2ω, and the fourth harmonic wave 4ω. The residual green light is filtered-out by a dichroic mirror (DM1) right after the second BBO crystal. The ω, 4ω beams are co-linearly incident on the third type-I phase-matched BBO

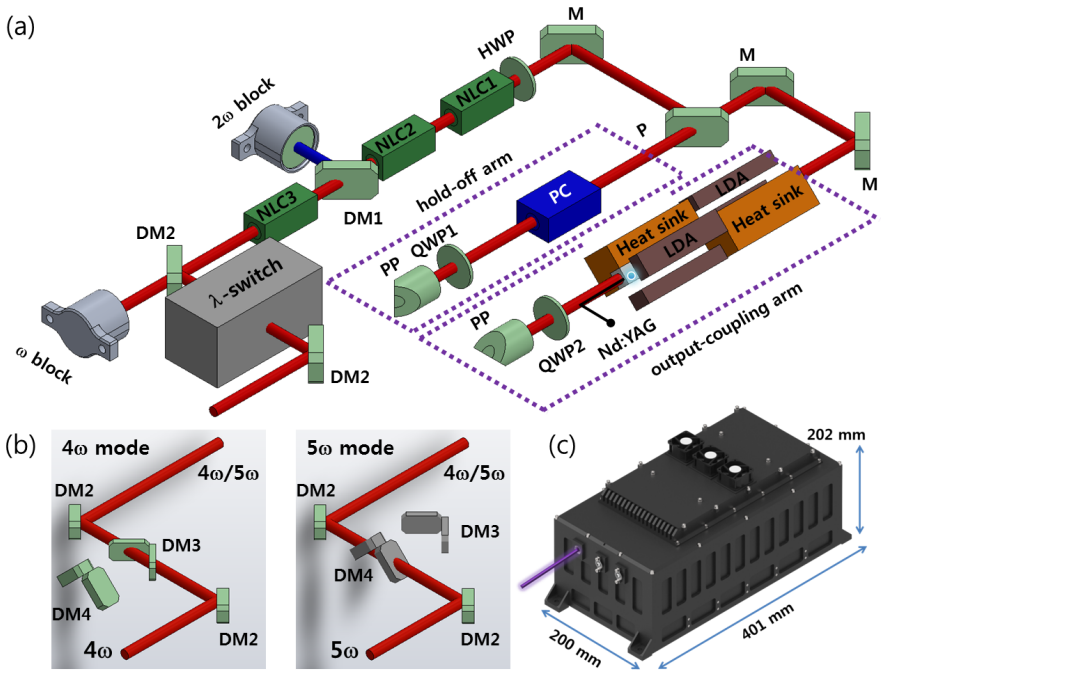

FIG. 1. (a) Experimental schematic of the pulsed Nd:YAG laser at mid-ultraviolet. PP, Porro prism; M, mirror; P, polarizer; QWP, quarter-wave plate; HWP, half-wave plate; PC, Pockels cell; DMs, dichroic mirrors; NLC, non-linear crystal; λ-switch, wavelength switch. (b) Details in the wavelength-switch. The output wavelength is selected to be 213 nm or 266 nm by a motorized linear stage. (c) The exterior of the UV laser with the dimensions of 200(W) × 401(L) × 202 (H) mm^3 and the weight of 11 kg including the power supply as well as the control electronics.

crystal yielding 213 nm (5ω) beam. Both surfaces of the third BBO crystal are AR coated at three waves, i.e. ω, 4ω, and 5ω. The 5th harmonic wave and the unconverted waves at 266 nm together with 1064 nm are coupled to the wavelength-selection-stage. The polarization of the ω, 4ω, and 5ω waves are p-wave, p-wave, and s-wave for the incidence plane, respectively. For stable operation the temperatures of the nonlinear crystals are independently controlled by the thermoelectric cooler (TEC). In particular, the phase-matching temperature of the 3rd BBO crystal is changed to vary the output energy ratio of the 5ω to the 4ω on demand without change of the output pulse parameters, e.g. the width as well as the shape. The fundamental wave is transmitted through the DM2, and the only harmonic waves at 4ω and the 5ω are reflected by the dichroic mirror 2(DM2) into the wavelength-switch (λ-switch) which is described in Fig. 1(b) in more detail.

The operation mode of the λ-switch is controlled by a motorized stage as shown in the Fig. 1(b) [23]. In the 4ω mode, the photons at 5ω and 4ω are reflected and transmitted, respectively, by the pair of the dichroic mirrors (DM3). In the 5ω mode, the UV beam at 213 nm is transmitted, while the UV light at 266 nm is reflected. The total transmission at 5ω and 4ω in the 5ω mode (4ω mode) is 0.810(0.000) and 0.001(0.942), respectively. Neither UV beam experiences any deviation in the beam path enabled by a pair of identical dichroic mirrors. The UV beams are finally reflected by another DM2 into the output window. The exterior of the UV laser is shown in Fig. 1(c). The dimensions are measured to be 200(W) × 401(L) × 202(H) mm^3 and the weight is estimated to be 11 kg including the power supply as well as the control electronics.

The output energy at the fundamental wave as a function of the pump energy is shown in Fig. 2. The slope efficiency and the maximum output energy are obtained to be 33% and 153 mJ per pulse, respectively, with a 0.22% RMS energy stability for the pump energy of 816 mJ. The output energy is varied with the slope of 0.3 mJ/°C in the operating temperature range of chemical reconnaissance vehicles showing excellent environmental reliability thanks to the crossed Porro prism resonator. The inset of Fig. 2 shows the measured pulse shape with the full-width at half-maximum (FWHM) of 21 ns yielding the maximum peak power of 7.3 MW.

The inset of Fig. 3 shows the beam profile of the fundamental wave at the output energy of 137 mJ. When the laser operates at a repetition rate of 20 Hz, we don't observe any distortion in the beam profile due to thermally induced effects in the laser rod [22] and any sudden intensity peak which can induce hotspot damage in the laser optics. In the beam profile, a subtle Maltese cross shape is shown, which might be due to slight thermal birefringence. For the average power of 16 W, the thermal birefringence is estimated to be 0.14λ indicating a weak thermal birefringence. The focal length of the thermal lens is deduced to be 14 m, which can be negligible [24]. The FWHM of the beam in the horizontal and vertical directions is deduced to be 3.5 mm and 3 mm, respectively. The M-squared of the fundamental beam is measured as shown in Fig. 3. The dotted rectangular (circle) is the measured width of the infrared beam as a function of the distance for the horizontal (vertical) direction. The M-squared values in the horizontal and the vertical directions are deduced to be 2.4 and 1.7, respectively. The slight discrepancy between the M-squared values in the horizontal and the vertical directions might be attributed to asymmetric cooling structure of the gain medium in the pumping head as shown in Fig. 1(a).

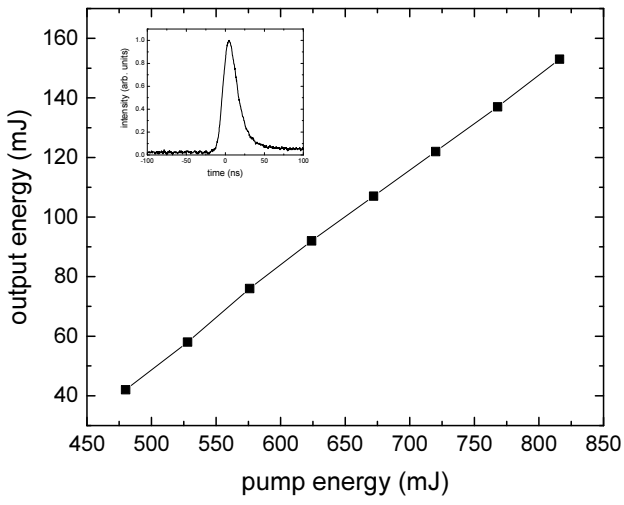

FIG. 2. The output energy per pulse at 1064 nm as a function of the pump energy. The slope efficiency is estimated to be 33%. Inset, the measured pulse shape with the FWHM of 21 ns.

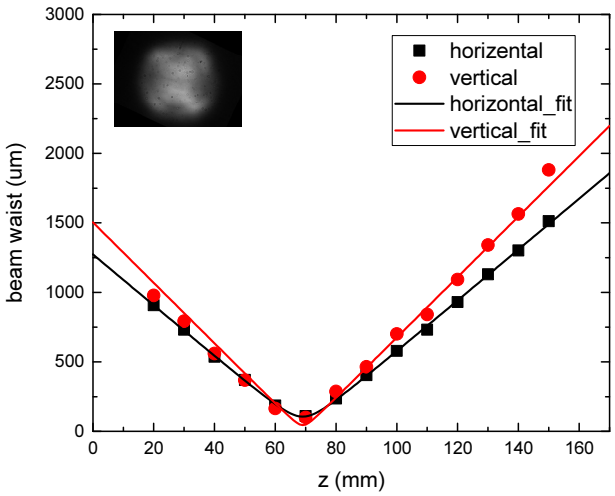

FIG. 3. The measured width of the infrared beam as a function of the distance for the horizontal (the vertical) direction. The M-squared in horizontal and vertical direction are deduced to be 2.4 and 1.7, respectively. Inset, the observed beam profile of the fundamental beam.

Figure 4 shows the measured harmonic energy (black rectangles for 2ω, red circles for 4ω, blue triangles for 5ω) and the calculated energy (black line for 2ω, red line for 4ω, blue line for 5ω) as a function of the pumping energy at the fundamental wave showing excellent agreement by the SNLO program, which is based on Maxwell equations integrated by split-step methods [25-28]. The maximum energy of each harmonic wave is 46.3 mJ, 15.1 mJ with a 0.92% RMS stability, and 6.8 mJ with a 1.03% RMS stability at 2ω, 4ω, and 5ω, respectively, leading to the conversion efficiency of 34%, 11%, and 5% for the fundamental wave energy. The discrepancy between the theoretical and the measured harmonic energies may be attributed to the increase of ellipticity of the linearly polarized fundamental beam wave as well as to weak distortion of beam shape due to thermal birefringence of the Nd:YAG rod in the high pumping energy regime.

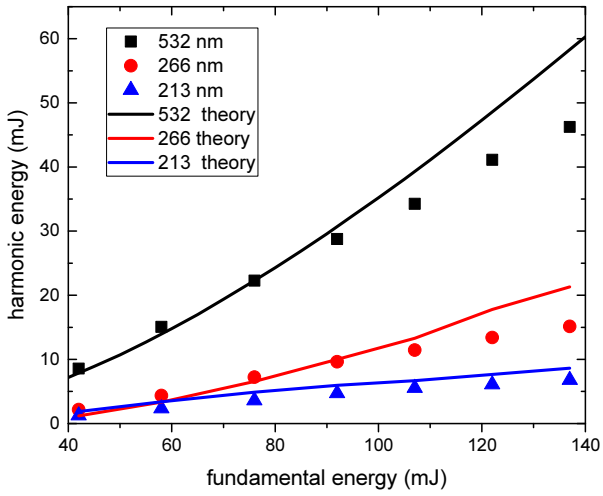

FIG. 4. The measured harmonic energy (black rectangles for 2ω, red circles for 4ω, blue triangles for 5ω) and the calculated energy (black line for 2ω, red line for 4ω, blue line for 5ω) by SNLO program as a function of the pumping energy at the fundamental wave.

The output wavelength is selected for 213 nm and 266 nm on demand as shown in Fig. 5(a). We don't observe any cross-talk in each wavelength mode. The energy ratio at 5ω to the 4ω is changed from 0.05 to 0.85 by varying the phase-matching temperature for the 3rd nonlinear crystal as shown in Fig. 5(b). The red line is calculated energy ratio by the SNLO program exhibiting good agreement.

III. CONCLUSION

We demonstrated a compact, wavelength-selectable Q-switched Nd:YAG laser at mid ultraviolet for chemical warfare agent detection. The fundamental wave at 1064 nm was delivered by a Q-switched solid state laser interfacing with a square-type Nd:YAG rod in a resonator closed by two crossed Porro prisms for environmental reliability. The maximum output energy achieved per pulse was 153 mJ with a slope efficiency of 33%. The beam quality factors in the horizontal and the vertical directions are deduced to be 2.4 and 1.7, respectively. The converted energy at 5ω and 4ω by $\chi^{(2)}$ process in the BBO crystals were measured to be 6.8 mJ and 15.1 mJ, respectively, by sequentially

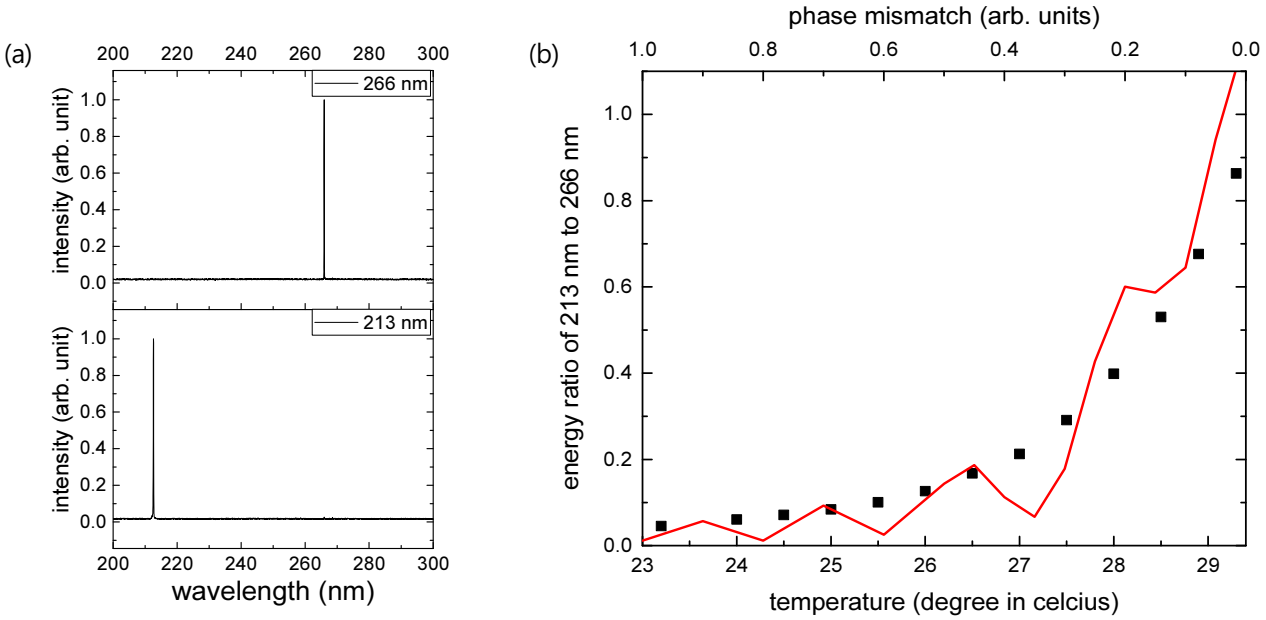

FIG. 5. (a) The output wavelength selection for 213 nm and 266 nm. (b) The measured variation of the energy ratio (black rectangular) at 5ω to the 4ω by controlling the phase-matching temperature for the 3rd nonlinear crystal. The red line is calculated energy ratio by the SNLO program.

disposing the nonlinear crystals. The output wavelength was selected for 5ω and 4ω by a motorized wavelength switch. The energy ratio of the 5ω to the 4ω was varied from 0.05 to 0.85 by controlling phase matching temperature of the nonlinear crystal for the sum-frequency generation on demand without change of the output pulse parameters, e.g. the width as well as the shape.

ACKNOWLEDGMENT

This work was funded and supported by the Agency for Defense Development.

REFERENCES

1. D. B. Coyle, R. B. Kay, P. R. Stysley, and D. Poulios, "Efficient, reliable, long-lifetime, diode-pumped Nd:YAG laser for space-based vegetation topographical altimetry," Appl. Opt. **43**, 5236-5242 (2004).
2. D. Carr and G. Tuell, "Estimating field-of-view loss in bathymetric lidar: application to large-scale simulations," Appl. Opt. **53**, 4716-4721 (2014).
3. B. Tan, "Deep microhole drilling in a silicon substrate using multi-bursts of nanosecond UV laser pulses," J. Micromech. Microeng. **16**, 1-4 (2006).
4. A. Bertsch, H. Lorenz, and P. Renaud, "3d microfabrication by combining microstereolithography and thick resist UV lithography," Sens. Actuators, A **73**, 14-23 (1999).
5. J. Kim, D. Haubrich, and D. Meschede, "Efficient sub-Doppler laser cooling of an indium atomic beam," Opt. Express **17**, 21216-21221 (2009).
6. A. Okamoto, H. Kuniyasu, and T. Hattori, "Detection of 30-40 nm particles on bulk -silicon and SOI wafers using deep UV laser scattering," IEEE Trans. Semicond. Manuf. **19**, 372-380 (2006).
7. R. T. Rewick, M. L. Schumacher, and D. L. Haynes, "UV absorption spectra of chemical agents and simulants," Appl. Spectrosc. **40**, 152-156 (1986).
8. S. D. Christesen, "Raman cross sections of chemical agents and simulants," Appl. Spectrosc. **42**, 318-321 (1988).
9. V. Pajcini, C. H. Munro, R. W. Bormett, R. E. Witkowski, and S. A. Asher, "UV Raman microspectroscopy: Spectral and spatial selectivity with sensitivity and simplicity," Appl. Spectrosc. **51**, 81-86 (1997).
10. R. Bhartia, W. F. Hugb, and R. D. Reid, "Improved sensing using simultaneous deep UV Raman and fluorescence detection," Proc. SPIE **8358**, 83581A (2012).
11. S. Jin, Z. Feng, F. Fan, and C. Li, "UV Raman spectroscopic characterization of catalysts and catalytic active sites," Catal. Lett. **145**, 468-481 (2015).
12. Y. C. Ha, J. H. Lee, Y. J. Koh, S. K. Lee, and Y. K. Kim, "Development of an ultraviolet Raman spectrometer for standoff detection of chemicals," Curr. Opt. Photon. **1**, 247-251 (2017).
13. S. D. Christesen, J. P. Jones, J. M. Lochner, and A. M. Hyre, "Ultraviolet raman spectra and cross-sections of the G-series nerve agents," Appl. Spectrosc. **62**, 1078-1083 (2008).
14. F. Kullander, L. Landström, H. Lundé, A. Mohammed, G. Olofsson, and P. Wästerby, "Measurements of Raman scattering in the middle ultraviolet band from persistent chemical warfare agents," Proc. SPIE **9073**, 90730C (2014).
15. W. R. Bosenberg, L. K. Cheng, and C. L. Tang, "Ultraviolet optical parametric oscillation in β-BaB_2O_4," Appl. Phys. Lett. **54**, 13-15 (1989).
16. R. B. Bapna, C. S. Rao, and K. Dasgupta, "Low-threshold operation of a 355-nm pumped nanosecond β-BaB_2O_4 optical parametric oscillator," Opt. Laser Technol. **40**, 832-837 (2008).
17. F. Kullander, L. Landström, H. Lundé, and P. Wästerby, "Experimental examination of ultraviolet Raman cross sections of chemical warfare agent simulants," Proc. SPIE **9455**, 94550S (2015).
18. M. K. Chun and E. A. Teppo, "Laser resonator: an electro-optically Q-switched Porro prism device," Appl. Opt. **15**, 1942-1946 (1976).
19. I. Singh, A. Kumar, and O. P. Nijhawan, "Design of a high-power Nd:YAG Q-switched laser cavity," Appl. Opt. **34**, 3349-3351 (1995).
20. A. Rapaport, L. Weichman, B. Brickeen, S. Green, and M. Bass, "Laser resonator design using optical ray tracing software: comparison with simple analytical models and experimental results," IEEE J. Quantum Electron. **37**, 1041-1048 (2001).
21. K. Lee, Y. Yoon, J. Lee, K. Cho, J. Kim, and J. Cho, "Linearly aligned multiple pumping apparatus for solid-state solid lasers," KR Patent 10-2018-0106942 (2018).
22. Y. Yoon, K. Cho, K. Lee, J. Yoo, J. Lee, J. Kim, S. Lee, and P. Jung, "Laser gain medium assembly solid-state solid lasers and assembling method thereof," KR Patent 10-2019-0001547 (2019).
23. Y. Ha, J. Lee, Y. Kang, K. Cho, J. Kim, and J. Cho, "High-order harmonic wave generation apparatus capable of selecting wavelength," U.S. Patent US9620927B2 (2017).
24. W. Koechner, *Solid-State Laser Engineering* (Springer-Verlag, 1996).
25. SNLO Program, http://www.as-photonics.com/snlo.
26. J. P. Phillips, S. Banerjee, J. Smith, M. Fitton, T. Davenne, K. Ertel, P. Mason, T. Butcher, M. Vido, J. Greenhalgh, C. Edwards, C. H. Gomez, and J. Collier, "High energy, high repetition rate, second harmonic generation in large aperture DKDP, YCOB, and LBO crystals," Opt. Express **24**, 19682-19694 (2016).
27. A. V. Smith and M. Bowers, "Phase distortions in sum- and difference-frequency mixing in crystals," J. Opt. Soc. Am. B **12**, 49-57 (1995).
28. A. V. Smith, W. J. Alford, T. D. Raymond, and M. S. Bowers, "Comparison of a numerical model with measured performance of a seeded, nanosecond KTP optical parametric oscillator," J. Opt. Soc. Am. B **12**, 2253-2267 (1995).